PHYSICAL REVIEW LETTERS

Oscillatory Optical Response of an Amorphous Two-Dimensional Array of Gold Nanoparticles

Tomasz J. Antosiewicz,[*] S. Peter Apell, Michael Zäch, Igor Zorić, and Christoph Langhammer[†]

Chalmers University of Technology, Department of Applied Physics, SE-412 96 Göteborg, Sweden
(Received 7 May 2012; published 12 December 2012)

The optical response of metallic nanoparticle arrays is dominated by localized surface plasmon excitations and is the sum of individual particle contributions modified by interparticle coupling that depends on specific array geometry. We demonstrate a so far unexplored distinct oscillatory behavior of the plasmon peak position, full width at half maximum, and extinction efficiency in large area *amorphous arrays* of Au nanodisks, which depend on the minimum particle center-to-center distance in the array. Amorphous arrays exhibit short-range order and are completely random at long distances. In our theoretical analysis we introduce a *film of dipoles* approach, within the framework of the coupled dipole approximation, which describes the array as an average particle surrounded by a continuum of dipoles with surface densities determined by the pair correlation function of the array.

Strong coupling of light to metal nanoparticles via localized surface plasmon resonances is one reason for the wide exploitation of nanosized metallic entities [1–4]. For many targeted uses of nanoplasmonic systems, a key question is whether to operate with individual metallic structures [5,6] or to use ensembles in the form of periodic [7] or random arrays on a support [8]. The optical properties of nanoplasmonic arrays, both periodic and fully random, stem from the optical response of individual particles. The array modifies these single-particle spectra, sometimes quite considerably, via interparticle coupling that depends on the exact array geometry.

Here we scrutinize experimentally and theoretically, by means of a *film of dipoles* approach in the framework of the coupled dipole approximation, a so far unexplored oscillatory behavior of the optical response from a specific type of nanoparticle array, somewhere between perfectly periodic and fully random, that we refer to as an *amorphous* array. This particular type of nanoparticle arrangement on a surface exhibits short range distance order while at long distances it is completely random. Furthermore, it can be quite easily fabricated on large areas (wafer scale), using bottom-up self-assembly based nanofabrication techniques like hole-mask colloidal lithography [9], making it a first choice for many large-scale devices and applications [2,10–13]. In contrast to earlier observations made on amorphous arrays of plasmonic nanoparticles for a limited particle density range [14], where the optical properties were attributed to a single particle optical response, our findings indicate that amorphous arrays exhibit distinct properties of interacting particles even if their density is low. This provides a powerful handle for tuning localized surface plasmon resonances, notably at *constant* particle size, shape, and material, in the myriad of documented applications of nanoplasmonics, which include bio- or chemosensing [2,15], light harvesting [3], photocatalysis [4], and surface enhanced spectroscopy [16,17].

For our experiments, we fabricated large area arrays of gold nanodisks with engineered randomness (to mimic arrays obtained by self-assembly techniques such as hole-mask colloidal lithography [9]) using a recently developed electron beam lithography nanofabrication scheme [8] as described in detail in the Supplemental Material [18]. Circular areas of roughly 30 mm^2 were patterned for each considered center-to-center (CC) distance with minimum imposed CC ranging from 2.5 to 7 in units of particle diameter D ($\mathcal{C}$). The size distribution for the disks is very narrow (as can be seen in Fig. 1, the Supplemental Material [18], and the histograms in Ref. [8]) and, consequently, basically eliminates inhomogeneous broadening. We fabricated large arrays with a very large number of particles to eliminate the possibility that for the same set of global parameters (minimum CC, D, thickness 20 nm, illumination conditions fixed) small samples could give rise to slightly different array realizations. Optical extinction measurements were carried out in a Cary 5000 spectrophotometer by measuring optical transmission in forward direction. During the experiment a circular nanopatterned area, defined by a pinhole with a radius of 2.5 mm, was illuminated at normal incidence by monochromatic light.

In the first two panels of Fig. 1, we present experimentally measured extinction efficiency spectra near the resonance to illustrate the sensitivity of the peak position and extinction efficiency per particle at peak to the CC value $\mathcal{C}$ for $D = 160$ nm in (a) and $D = 260$ nm in (b). In a first rough analysis for $D = 160$ nm, we see that for $\mathcal{C} = 2.5$ extinction is maximal at 838 nm, then it redshifts for $\mathcal{C} = 3$ and 4 to 855 and 867 nm, respectively, and then undergoes a blueshift to 837 nm ($\mathcal{C} = 5$) and 815 nm for $\mathcal{C} = 6$. This suggests an oscillatory behavior of the peak position. A similar trend is also seen when tracing the peak amplitude (extinction efficiency) and the linewidth. Such oscillations in plasmon frequency have not been observed in earlier studies of *ordered* arrays that focused on the influence of particle
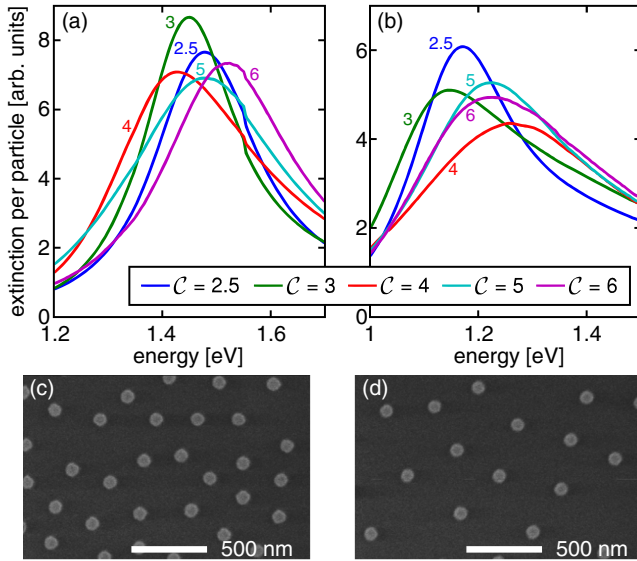
FIG. 1 (color online). Experimentally measured extinction spectra of gold nanodisks with an engineered randomness. Resonance position, peak value, and linewidth all show a nonmonotonic dependence on lattice parameter $\mathcal{C}$ being minimum center-to-center distance in units of disk diameter D: (a) $D = 160$ nm, (b) 260 nm. (c) and (d) show SEM images of the amorphous arrays for $\mathcal{C} = 3$ and 4, respectively. Notice the random distribution of perfectly defined particles.

spacing on array spectra [19–21]. A double-peaked structure of the resonance position in Ref. [19] was attributed to two different conditions for the emergence of the first diffraction order—one into the substrate and one into air.

An efficient way to model arrays of plasmonic nanoparticles is by a coupled dipole approximation in which each disk is modeled by an induced point dipole coupled to an external electromagnetic field [22]. In this framework, the particle properties are described by a polarizability α determined by the material, geometry, and surrounding medium [23,24]. In the quasistatic regime, the polarizability α_{qs} is proportional to $V(\epsilon_m - \epsilon_s)/[\epsilon_s + L(\epsilon_m - \epsilon_s)]$, where ϵ_m and ϵ_s are the permittivities of the metal particle and surrounding medium, respectively, V is the particle volume, and L is a shape depolarization factor. Dynamic depolarization and radiative damping are accounted for by introducing the modified long wavelength approximation (MLWA) [24,25] $1/\alpha = 1/\alpha_{qs} - \frac{2}{3}ik^3 - \frac{k^2}{a}$, where k is the wave number of exciting light of wavelength λ and a is a length associated with the particle geometry [24]. The nanodisks considered here, despite their relatively large sizes, are adequately described by a dipolar MLWA in view of the diameter-to-plasmon-wavelength ratios of $\frac{1}{3}$ to $\frac{1}{4}$, which are in the same range as in earlier MLWA studies for similar-sized particles [20,21]. The dipolar nature of the plasmon resonance in Au nanodisks in the same size range was furthermore confirmed experimentally in a recent study by Khunsin *et al.* [26].

For an infinite periodic array, where the particles are interacting, the system of coupled equations is solved by assuming

that the polarization of each particle is the same and thus α becomes an effective polarizability that takes into account interparticle interactions via a retarded dipole sum [7,27,28].

For an *amorphous* array, we can, as an ensemble average, define an effective polarization α^*. One way of analyzing the interparticle contributions to α^* is to average over many realizations of amorphous arrays (i.e., dipole sums). Here, however, we introduce a model in which the average particle is surrounded by a continuous *film of dipoles* with surface densities determined by the pair correlation function $\mathcal{G}(r, \mathcal{C})$, where r is the radial distance from the considered particle. One can think of this as an average of an infinite number of different realizations of amorphous arrays centered around a specified particle placed at a particular specified point. In a sense this approach is reminiscent of the coherent-potential approximation for a random distribution of particles on a square array [29] or a field averaging scheme [30].

For the average particle in an amorphous array, we carry out the same procedure of solving the discrete dipole equations as in Ref. [27] where the retarded dipole sum (discrete particles) is replaced by a retarded dipole integral (continuous film with hole)

$$S(\mathcal{C}) = \int_{\ell_{CC}}^{+\infty} \int_0^{2\pi} e^{ikr} \left[\frac{(1-ikr)(3\cos^2\theta - 1)}{r^3} + \frac{k^2\sin^2\theta}{r} \right] \times g(r, \mathcal{C}) r \, d\theta \, dr, \tag{1}$$

where the exponential term multiplied by the expression in the square brackets ($e^{ikr}[\ldots]$) describes the retarded dipole-dipole interaction, $g(r, \mathcal{C}) = \sigma \mathcal{G}(r, \mathcal{C})$ is the pair correlation function $\mathcal{G}(r, \mathcal{C})$ multiplied by the particle surface density $\sigma = \sigma_0 \ell_{CC}^{-2}$, $\ell_{CC} \equiv \mathcal{C}D$, and σ_0 is a surface packing parameter. The integration is over the whole 2D (r, θ) space with the exception of an inner circle smaller than ℓ_{CC}. Performing the angular integration yields the average, effective polarizability [7,27]

$$\alpha^* = \frac{1}{\alpha^{-1} - \mathcal{S}}, \tag{2}$$

where

$$\mathcal{S} = \pi\sigma \int_{\ell_{CC}}^{+\infty} e^{ikr} \left(k^2 + \frac{1 - ikr}{r^2} \right) \mathcal{G}(r, \mathcal{C}) dr. \tag{3}$$

The function $e^{ikr}[k^2 + (1 - ikr)/r^2]$ consists of two parts: the first ($e^{ikr}k^2$) comes from the far-field dipole radiation and its value oscillates, while the second [$e^{ikr}(1 - ikr)/r^2$] corresponds to intermediate and near fields and its value has a well-defined limit for $r \to \infty$. However, these observations are only strictly valid for a well behaved function $\mathcal{G}(r, \mathcal{C})$ at infinity.

To perform the integration for $\mathcal{S}$ in Eq. (3) we require an expression for $\mathcal{G}(\rho, \mathcal{C})$, where $\rho = r/D$ is a normalized radius. We obtain $\mathcal{G}(\rho, \mathcal{C})$ by finding a function which fits well ($R^2 \simeq 1$) to pair correlation data calculated from random distributions of particles generated with the random sequential adsorption algorithm, which was also used to calculate particle positions for the fabricated arrays [31]. The selected function consists of two parts—a constant and a varying one

$$\mathcal{G}(\rho, \mathcal{C}) = 1 + \sin\left(2\pi\frac{\rho - d_0\mathcal{C}}{d_1\mathcal{C}}\right)[a_0 e^{-a_1\mathcal{C}^{a_2}(\rho - c\mathcal{C})}$$
$$+ b_0 e^{-b_1\mathcal{C}}e^{-b_2\mathcal{C}^{b_3}(\rho - c\mathcal{C})}] \quad \text{for } \rho \geq \mathcal{C}. \quad (4)$$

It is chosen because its product with functions describing dipole fields is relatively easy to compute and its $R^2 = 0.99$ (fitting parameters given in Ref. [32] and more information is given in the Supplemental Material [18]). Slight differences between this function and the one shown by Hinrichsen *et al.* [31] occur only for particles at close distances. However, as we show later, a qualitative description is insensitive to the exact expression describing the short range order.

Equation (4), while easily integrable when multiplied by the electric dipole field [33], does not lend itself to an easy exposition of the main physics taking place. Therefore, a qualitative analysis is carried out first, before performing the full calculation. We do this by keeping the hard-core part (unity) and omitting the second, oscillating term (multiplied by the sine function). Thus, the simplified $\mathcal{G}$ reduces to a Heaviside step function $\Theta(\rho - \mathcal{C})$ that describes a fully random array with a removed circle of radius $\mathcal{C}$ around the average particle. The simplification still describes satisfyingly the most important property of the array, namely, the short-range order defined by the minimal allowed CC distance for the analyzed particle, and does not alter the main physical processes occurring within the array.

The function $\mathcal{G} = \Theta(\rho - \mathcal{C})$ is derived from Eq. (4) by setting the pair correlation function to unity. To calculate the far-field term, which oscillates around a mean value, we modify it by adding to the exponent the term $-\varepsilon r$, which makes the expression $\pi\sigma k^2\int_{\ell_{CC}}^{+\infty}e^{ikr-\varepsilon r}dr$ well defined. This represents a case when the array is illuminated by a very broad Gaussian beam; i.e., disks very far away from the center of the beam feel a diminished intensity of the electric field, but the decay is slow enough that the average treatment of the disks holds.

The first integral in $\lim_{\varepsilon\to 0}$ equals $\pi\sigma kie^{ik\ell_{CC}}$ and the second $\pi\sigma e^{ik\ell_{CC}}/\ell_{CC}$. Thus, for the simplified case of $\mathcal{G} = \Theta(\rho - \mathcal{C})$, the retarded dipole integral becomes

$$\mathcal{S}^\Theta = \pi\sigma\frac{e^{ik\ell_{CC}}}{\ell_{CC}}(1 + ik\ell_{CC}). \quad (5)$$

We substitute this result into the effective polarizability α^* [Eq. (2)] and rewrite the right-hand side containing the substituted expressions into a Lorentzian form to easily identify the peak position and full width at half maximum (FWHM). We employ, as an illustrative *test case*, a generic metal sphere with a Drude dielectric function $\epsilon(\omega) = 1 - \omega_p^2/[\omega(\omega + i\gamma)]$. Using the MLWA, we get

$$\frac{\alpha^*}{4\pi\epsilon_0 R^3} = \frac{1 - \bar{\omega}^2(1 + s^2) - qf + i[\bar{\omega}(\bar{\gamma} + \frac{2}{3}s^3\bar{\omega}^2) + qg]}{[1 - \bar{\omega}^2(1 + s^2) - qf]^2 + [\bar{\omega}(\bar{\gamma} + \frac{2}{3}s^3\bar{\omega}^2) + qg]^2}, \quad (6)$$

where we have introduced dimensionless variables $\bar{\omega} \equiv \omega/\omega_0$, $\bar{\gamma} \equiv \gamma/\omega_0$, $s \equiv \omega_0 R/c$ with $\omega_0^2 = \omega_p^2/3$ the Mie resonance frequency, a coupling strength $q \equiv \pi\sigma_0(R/\ell_{CC})^3$

(q is maximum $\frac{\pi}{4}$ for $\sigma_0 = 1$), two functions $f(k\ell_{CC})$ and $g(k\ell_{CC})$: $f(x) = \cos x - x\sin x$, $g(x) = \sin x + x\cos x$, and c is the speed of light.

From the denominator of Eq. (6) we can read off the resonance frequency and the FWHM. In the noninteracting case ($q = 0$), we have a mode at $\bar{\Omega}_N = 1/\sqrt{1 + s^2}$ with a linewidth $\bar{\Gamma}_N = (2/\sqrt{1 + s^2})(\bar{\gamma} + [2s^3/3(1 + s^2)])$. For an amorphous array consisting of such particles the resonance is modified by interparticle coupling via the retarded dipole integral and Eq. (6) shows that we have a resonance at

$$\bar{\Omega}_I/\bar{\Omega}_N = \sqrt{1 - qf(k_N\ell_{CC})}, \quad (7)$$

in terms of the noninteracting $\bar{\Omega}_N$ and a linewidth of

$$\bar{\Gamma}_I/\bar{\Gamma}_N = 1 + 2(1 + s^2)Q_N g(k_N\ell_{CC}), \quad (8)$$

where Q_N is the individual particle quality factor defined as the ratio of the peak position and its width. We see from Eqs. (7) and (8) that due to the quality factor we expect the randomness to show up much more in the FWHM than in the resonance frequency. This is clearly seen in Fig. 2 which shows peak position (solid) and FWHM (dashed) based on Eqs. (7) and (8). The peak position follows a sinusoidal line with a period determined by the ratio of the minimum particle-particle distance to the resonance wavelength λ_N of a single particle. Notice, that the oscillations are governed by the low cutoff ℓ_{CC}. The real part of the dipole interaction term shifts the resonance position towards higher frequency when $\Re(\mathcal{S}) \equiv f < 0$, while for $\Re(\mathcal{S}) > 0$ it induces a red shift. The largest shifts occur when the array is relatively dense, cf. large coupling strength q. For large interparticle spacing the interference between the disks vanishes since q is proportional to ℓ_{CC}^{-3}.
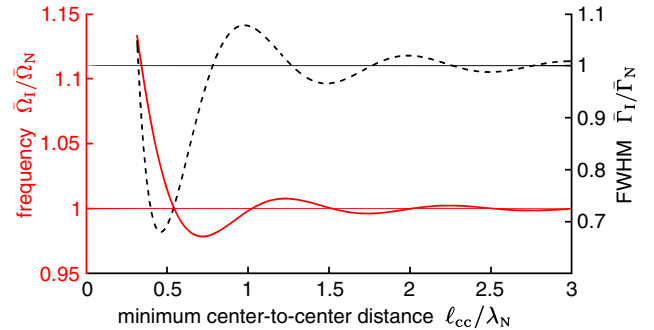

FIG. 2 (color online).   The variation of the optical characteristics of the particle arrays in Fig. 1 can be understood from a simple generic Drude model. The resonance frequency (solid) and FWHM (dashed) of the array using a hard core pair-correlation function with minimum center-center distance ℓ_{CC} is shown. We measure the center-center distance ℓ_{CC} in units of the resonance wavelength λ_N. The resonance frequency as well as the linewidth are in units of the bare particle properties. Notice how the interference between the particles causes both resonance frequency and FWHM to oscillate and the oscillations of the FWHM are larger than for the resonance frequency. With decreased coupling, the curves settle to the single particle values.

The single particle resonance linewidth $\bar{\Gamma}_I$ is modified by the imaginary part of $\mathcal{S}^\Theta \equiv g$ which introduces a modulation of the linewidth equal to $(1 + s^2) Q_N g(k_N \ell_{CC})$. Similar to the peak position, the linewidth is a decaying oscillatory function that tends to the single particle resonance width for infinitely diluted amorphous arrays. When $g < 0$ for even-numbered half-periods the resonance linewidth is smaller than the single particle one; however, it does not go to zero [24,34–36]. Note, that in this analysis we have kept the minimum center-center distance larger than that of the order of two diameters so that higher order multipoles which are not present in the theory should be negligible.

In the above *qualitative* picture, in which we dropped the oscillatory term in the pair correlation function, we have shown that the oscillations of the optical cross sections of amorphous arrays are the result of interference between the incident field driving a particle and the scattered fields originating from the other particles in the array. We use now the full expression for $\mathcal{G}$ [Eq. (4)] to analyze experimental data, shown in Fig. 1, obtained from extinction measurements on nanofabricated amorphous arrays of nanodisks. To model the properties of a single disk in the array, we adjust an oblate spheroidal polarizability so that the single disk (for a hypothetical case of an infinitely diluted array) resonance position and linewidth correspond to the asymptotes of the experimental arrays for very large CC.

First, we address the extinction cross sections per particle in the arrays. Figure 3(a) presents the measured and calculated extinction per disk in the array, C_e, normalized to the extinction of a single disk. Clearly, extinction exhibits strong oscillatory CC distance dependence for all three measured particle sizes. The minimum-to-maximum difference is about 40% for small CC distances and agrees very well with the model calculations.

The measured experimental peak positions (diamonds) and FWHM (circles) values are shown in Figs. 3(b)–3(d). The solid orange and dashed blue lines representing peak position and FWHM values, respectively, are calculated according to the scheme outlined above. The agreement between the theoretical and experimental data is reasonable in view of our relatively simple theoretical treatment of the particle interaction in the array. The period and phase shift of the measured and calculated oscillations of the peak position and FWHM are consistent and show a pronounced CC distance dependence. Notably, the experimentally measured FWHM for the $D = 260$ nm disk varies between ca. 0.3 and 0.5 eV at a rather moderate change of the peak position (1.15 to 1.25 eV). As analyzed in detail previously, the agreement between MLWA data for peak position, intensity, and FWHM and the experimental one for diluted amorphous arrays ($\mathcal{C} = 6$) is excellent [8], indicating the validity of our model for a reasonable quantitative description for the considered system, despite its simple nature.

We now briefly address trends in the amplitude of the oscillations that physically originate from radiative coupling as a function of nanodisk size in the amorphous array. It is
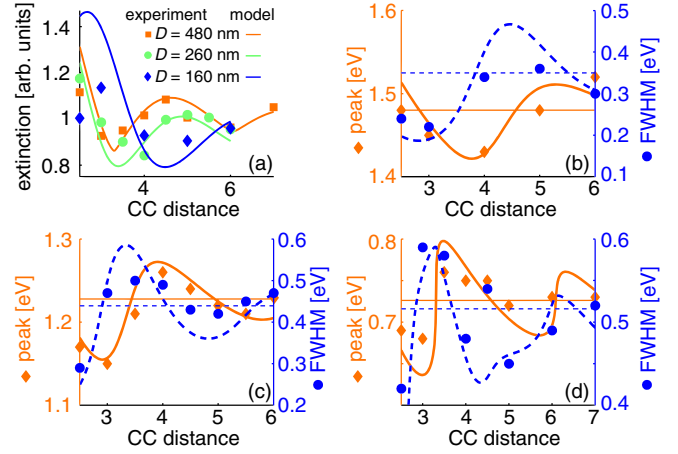

FIG. 3 (color online). Experimental results compared to our predictions based on the full pair-correlation function for the extinction at peak value, the peak position and linewidth as a function of the minimum particle-particle distance in units of particle diameter. The characteristics of the spectra (extinction value, position, and linewidth) oscillate as a result of radiative coupling between the plasmonic particles within the array and are a function of the minimum CC distance. (a) shows peak extinction values for a disk in the amorphous array for the different disk diameters, which are normalized to the peak extinction values of their respective single particles; (b)–(d) show extinction peak position (solid orange line, left y axis) and linewidth (dashed blue line, right y axis) for diameters (b) 160, (c) 260, and (d) 480 nm as a function of the CC distance. The horizontal thin solid and dashed lines indicate asymptotes of the peak position and linewidth of the amorphous arrays, respectively.

known from theory and experiment that the scattering efficiency, especially compared with absorption (i.e., the scattering-absorption branching ratio), increases with particle size [37]. Thus, it is to be expected that the oscillations are most pronounced for the largest particles, where the radiative coupling is strong, and decrease in amplitude as the nanodisk diameter decreases. This is precisely the trend that can be seen in Fig. 3 [for $D = 480$ nm, the maximum peak position oscillation amplitude (ΔE) normalized to peak position (E_0) is $\Delta E/E_0 = 0.11$, for $D = 260$ nm, $\Delta E/E_0 = 0.09$, and for $D = 160$ nm, $\Delta E/E_0 = 0.06$]. Consequently, the decrease of the oscillatory amplitude is expected to continue as the nanoparticle diameter further decreases. This can be clearly seen in Fig. 2, where a 60 nm Drude sphere was considered.

The observed discrepancies between the calculated values for the peak position and, in particular, the FWHM are the result of several factors, among which are inhomogeneity of the fabricated disks (this effect is, however, small), the fact that disks with large diameter-to-thickness ratios are not perfectly described by one dipole, and the estimation of the long-range interference term in the dipole integral. Another issue to be noted here is the illumination of the array in the modeling, i.e., the assumption of a very broad Gaussian beam incident onto an infinite amorphous array (the array is in focus, so the phase of the incident beam is uniform). The latter assumption is then used to calculate the far-field term. However, for a finite array this is not fully

correct. Far-field radiation is proportional to e^{ikr} and its definite integral (present in the retarded dipole integral) oscillates, so the value of the sum for a finite array depends on the exact relation between the array and the illumination. Thus, our result is to be viewed as an average value.

The occurrence of these oscillations has direct implications for plasmonic devices. For example, in plasmonic sensing applications a slight tuning of the CC distance in an amorphous array can significantly boost the figure of merit [38]. As a second example, the possibility of tailoring the peak linewidth in the near infrared spectral range is of particular interest in the surface enhanced infrared absorption spectroscopy [16,17], where broad resonances are sought to overlap with the sharp and localized vibrational excitations of adsorbed molecules. Thus, in view of its wide-ranging implications, our work provides a widely unexplored tool for optimizing the particle-light interaction in nanoplasmonic systems by tailoring the particle CC distance in amorphous plasmonic nanoparticle arrays.

In summary, we have shown experimentally and explained, using a film of dipoles model, an unexpected oscillatory optical response of amorphous plasmonic nanoparticle arrays that depends on the minimum allowed particle-particle separation. Optical spectra of amorphous arrays, while stemming from those of single particles, exhibit a strong influence of intra-array radiative coupling of the plasmonic disks that results in oscillation of the extinction, its position, and linewidth, which have not been observed in periodic arrays.

*tomasza@chalmers.se
†clangham@chalmers.se

[1] A. V. Kabashin, P. Evans, S. Pastkovsky, W. Hendren, G. A. Wurtz, R. Atkinson, R. Pollard, V. A. Podolskiy, and A. V. Zayats, Nat. Mater. **8**, 867 (2009).

[2] E. M. Larsson, C. Langhammer, I. Zorić, and B. Kasemo, Science **326**, 1091 (2009).

[3] H. A. Atwater and A. Polman, Nat. Mater. **9**, 205 (2010).

[4] S. Linic, P. Christopher, and D. B. Ingham, Nat. Mater. **10**, 911 (2011).

[5] A. D. McFarland and R. P. Van Duyne, Nano Lett. **3**, 1057 (2003).

[6] N. Liu, M. L. Tang, M. Hentschel, H. Giessen, and A. P. Alivisatos, Nat. Mater. **10**, 631 (2011).

[7] B. Auguié and W. L. Barnes, Phys. Rev. Lett. **101**, 143902 (2008).

[8] I. Zorić, M. Zäch, B. Kasemo, and C. Langhammer, ACS Nano **5**, 2535 (2011).

[9] H. Fredriksson, Y. Alaverdyan, A. Dmitriev, C. Langhammer, D. S. Sutherland, M. Zäch, and B. Kasemo, Adv. Mater. **19**, 4297 (2007).

[10] V. Gusak, B. Kasemo, and C. Hägglund, ACS Nano **5**, 6218 (2011).

[11] R. Esteban, R. Vogelgesang, J. Dorfmüller, A. Dmitriev, C. Rockstuhl, C. Etrich, and K. Kern, Nano Lett. **8**, 3155 (2008).

[12] B. Sepúlveda, J. B. González-Díaz, A. García-Martín, L. M. Lechuga, and G. Armelles, Phys. Rev. Lett. **104**, 147401 (2010).

[13] O. E. Daif, L. Tong, B. Figeys, K. Van Nieuwenhuysen, A. Dmitriev, P. Van Dorpe, I. Gordon, and F. Dross, Solar Energy Mater. Sol. Cells **104**, 58 (2012).

[14] P. Hanarp, M. Käll, and D. S. Sutherland, J. Phys. Chem. B **107**, 5768 (2003).

[15] J. N. Anker, W. P. Hall, O. Lyandres, N. C. Shah, J. Zhao, and R. P. Van Duyne, Nat. Mater. **7**, 442 (2008).

[16] R. Adato, A. A. Yanik, J. J. Amsden, D. L. Kaplan, F. G. Omenetto, M. K. Hong, S. Erramilli, and H. Altug, Proc. Natl. Acad. Sci. U.S.A. **106**, 19 227 (2009).

[17] S. Cataldo, J. Zhao, F. Neubrech, B. Frank, C. Zhang, P. V. Braun, and H. Giessen, ACS Nano **6**, 979 (2012).

[18] See Supplemental material at http://link.aps.org/supplemental/10.1103/PhysRevLett.109.247401 for experimental details, quantitative analysis of edge effects, and additional pair correlation function data.

[19] B. Lamprecht, G. Schider, R. T. Lechner, H. Ditlbacher, J. R. Krenn, A. Leitner, and F. R. Aussenegg, Phys. Rev. Lett. **84**, 4721 (2000).

[20] C. L. Haynes, A. D. McFarland, L. Zhao, R. P. Van Duyne, G. C. Schatz, L. Gunnarsson, J. Prikulis, B. Kasemo, and M. Käll, J. Phys. Chem. B **107**, 7337 (2003).

[21] L. Zhao, K. L. Kelly, and G. C. Schatz, J. Phys. Chem. B **107**, 7343 (2003).

[22] B. T. Draine and P. J. Flatau, J. Opt. Soc. Am. A **11**, 1491 (1994).

[23] C. Bohren and D. Huffman, *Absorption and Scattering of Light by Small Particles* (John Wiley & Sons, New York, 1983).

[24] A. Moroz, J. Opt. Soc. Am. B **26**, 517 (2009).

[25] T. Jensen, L. Kelly, A. Lazarides, and G. C. Schatz, J. Cluster Sci. **10**, 295 (1999).

[26] W. Khunsin, B. Brian, J. Dorfmüller, M. Esslinger, R. Vogelgesang, C. Etrich, C. Rockstuhl, A. Dmitriev, and K. Kern, Nano Lett. **11**, 2765 (2011).

[27] S. Zou and G. C. Schatz, J. Chem. Phys. **121**, 12 606 (2004).

[28] V. A. Markel, J. Phys. B **38**, L115 (2005).

[29] B. N. J. Persson and A. Liebsch, Phys. Rev. B **28**, 4247 (1983).

[30] M. Meier, A. Wokaun, and P. F. Liao, J. Opt. Soc. Am. B **2**, 931 (1985).

[31] E. L. Hinrichsen, J. Feder, and T. Jøssang, J. Stat. Phys. **44**, 793 (1986).

[32] The fitted parameters are $a_0 = 0.5055$, $a_1 = 1.445$, $a_2 = -1.445$, $b_0 = 3.619$, $b_1 = 0.003095$, $b_2 = 16.64$, $b_3 = -1.016$, $c = 0.991$, $d_0 = 2.019$, $d_1 = 1.185$.

[33] J. D. Jackson, *Classical Electrodynamics* (John Wiley & Sons, New York, 1999), Chap. 9, p. 411.

[34] S. Zou, N. Janel, and G. C. Schatz, J. Chem. Phys. **120**, 10 871 (2004).

[35] V. A. Markel, J. Chem. Phys. **122**, 097101 (2005).

[36] S. Zou and G. C. Schatz, J. Chem. Phys. **122**, 097102 (2005).

[37] C. Langhammer, B. Kasemo, and I. Zorić, J. Chem. Phys. **126**, 194702 (2007).

[38] M. Schwind, V. P. Zhdanov, I. Zorić, and B. Kasemo, Nano Lett. **10**, 931 (2010).